



Multipoint chord reference system for track irregularity: Part I – Theory and methodology



Yuan Wang^{a,b,d}, Huiyue Tang^{c,d}, Ping Wang^{a,b}, Xiang Liu^d, Rong Chen^{a,b,*}

^a School of Civil Engineering, Southwest Jiaotong University, Chengdu, China

^b Key Laboratory of High-speed Railway Engineering, Ministry of Education, Chengdu, China

^c School of Electrical Engineering, Southwest Jiaotong University, Chengdu, China

^d Department of Civil and Environmental Engineering, Rutgers, The State University of New Jersey, NJ, USA

ARTICLE INFO

Article history:

Received 23 June 2018

Received in revised form 23 January 2019

Accepted 26 January 2019

Available online 4 February 2019

Keywords:

Multipoint chord reference system, sensor fusion

Least square optimization

Track irregularity

Rail corrugation

Error amplification factor

ABSTRACT

This paper proposes a novel approach to measure track irregularity by using a multipoint chord reference (MCR) system. This paper is the first part presenting the theoretical proofs and methodology for analyzing the system performance in a spatial domain. Part II will study the performance in wavelength domain through numerical approaches. In this paper, a unified framework of the MCR system is introduced with a series of definitions. Mathematical models are established based on sensor fusion and least square optimization techniques. The error theory of the MCR system is discussed and the error amplification factor (EAF) is defined to quantify the error accumulation characteristics of the MCR system in the spatial domain. The stability of the MCR system was analyzed and propositions are put forward to reveal the basic relationship between the minimum measurable wavelength and different configurations. In particular, the MCR($n, 1$) system was studied, for which propositions were put forward to describe the relationship between the EAF and stability of the MCR system. The MCR system has significant advantages over some current techniques for track irregularity measurement, such as single point chord method as well as gyroscope- and accelerometer-based techniques. The MCR system enables us to use low-cost sensors to achieve the same or even higher precision as the currently used techniques by increasing the number of sensors and sampling frequency. This system can be especially useful to measure track irregularities with short wavelengths, such as rail corrugation. Although the MCR system is mostly used in the railway engineering field, it can be applied to any field in which an irregular surface or curve is required to be measured.

© 2019 Published by Elsevier Ltd.

1. Introduction

1.1. Background

The efficient and fast detection of track geometry irregularity, especially short wavelength irregularity such as rail corrugation [1–4], is of crucial importance to the smooth running, safety, and maintenance of both high-speed railway and urban railway transit [5–10].

Our previous publication [4] presented a detailed study on the error theory of the mid-chord offset method (MCO method). In this paper, we extend the single-point measurement method (a single sensor on the middle of a reference chord) to a multipoint chord measurement method, namely the multipoint chord reference sys-

tem (MCR system). We integrate the whole family of such chord-based measurement systems into one unified framework, namely the framework of the MCR system. This system has superior performance over currently used chord methods for the measurement of track irregularity, especially for short wavelength components, such as rail corrugation. The MCR system provides an approach to enhance the final precision and measure smaller wavelengths by adding more sensors or increasing the measurement frequency. It can also be used to reduce the measurement cost by using low precision sensors.

The measurement process of a chord-based system can be described in general as the referential use of a chord formed between two points on the rail and the measurement of the distance between this reference chord and a third position on the rail [4,5,9–13]. As mentioned in [4], according to a long existing misconception, the measured distance between the rail and reference chord (namely, the chord versine value) is considered as an

* Corresponding author at: School of Civil Engineering, Southwest Jiaotong University, Chengdu, China.

E-mail address: chenrong@home.swjtu.edu.cn (R. Chen).

approximating description of track geometry irregularity. This paper, again, emphasizes on the correction of this misconception by stating that the measured versine values are only signals storing the micro information of the track geometry to be measured and should not be used directly to describe the irregularity of track geometry. By using proper models and theoretical analyses, the original track geometry curve can almost perfectly be reconstructed based on the measured versine values [4].

1.2. Brief review of track irregularity measurement

Refs. [4,5,8,9] provide a detailed overview of the measurement techniques for track irregularity, in particular, for the measurement of medium or long wavelengths. This paper mainly focuses on measuring short-wavelength irregularity because for the measurement of short wavelengths, the inertial-reference measurement system [5] becomes useless. The MCO system [4] is also impractical for the measurement of short wavelengths. The methods that can be used for short wavelength measurement include (1) asymmetric three-point chord (ATC) system [5,14,15], (2) acceleration-based technique [5,9,16–20], and (3) indirect measurement, such as the use of noise [5,9,17] or axlebox acceleration [21–24]. A detailed introduction regarding acceleration-based technique and indirect measurement can be found in [1,5,16–18]. In the following text, we focus only on a chord-based system.

Initially, the MCO system was widely used [4,10–13], in which the reference chord, generally with a length of approximately 1 m, moves along the rail propelled by a trolley or vehicle to achieve a continuous measurement of rail geometry. Later, researchers found a drawback in the measurement process, during which the two ends of the reference chord always changed along the rail, leading to a variation (ranging from 0 to 2) of the amplitude transfer function [4,5,9–13]. For the MCO system, the zero points of amplitude repeat periodically, making it impossible for

those wavelengths to be measured, even by using a stronger model. As a countermeasure, the ATC system [14,15] was proposed as the transfer function was enhanced owing to the special distribution of zero points. However, as the phase of the ATC system is distorted [5,9,14,15], the restoration of the original waveform (known as the *decoloring* process [5]) becomes difficult and involves a long and complicated infinite impulse response filter-designing process [15]. Other filter-based approaches, such as deconvolution [25], particle filter [26], and adaptive Kalman filtering [27] have also been used to improve the performance of chord-based systems.

According to our knowledge, none of the current chord-based techniques considers a chord system with multiple measured points on the reference chord. Although Mao et al. [28] proposed a four-point chord method, the main contribution is the linear assembling of the measured versine values to improve the transfer function (zeros points), and then using Fourier Transform to realize the decoloring process. The principle used in [28] is conventional and the value of the measured data is far from fully functional.

1.3. Organization and relation between the studies in parts I and II

This study of the MCR system is divided into two parts, as presented in Fig. 1. Part I presents some basic definitions, essential models, and a case study of the MCR(*n*, 1) system. This part also focuses on the system performance in the spatial domain, and the methodology in use is mainly based on theoretical analysis. Part II provides definitions of some components in the wavelength domain, such as the transfer function and critical wavelength, and is focused on the performance in the wavelength domain, and the methodology in use is mainly based on numerical analysis.

The two parts are separated into two studies but are related. The organization and relation between Parts I and II are illustrated in Fig. 1. The main dependency relationships are highlighted by

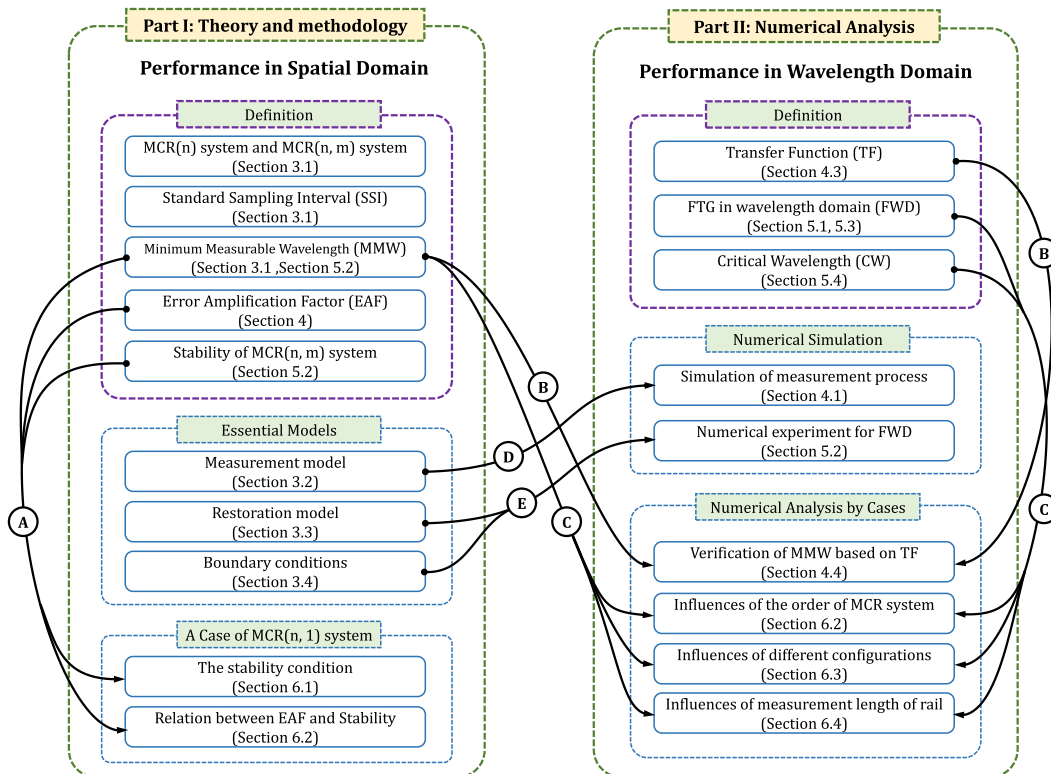


Fig. 1. Organization and relation between Part I and II studies. The main dependency relationships are highlighted by black arrow lines with circled letters A–E. The same letter indicates that the arrow lines should be combined.

black arrow lines, with circled letters A–E. The same letter indicates that the arrow lines should be combined.

1.4. Contributions of this paper

The contributions of this paper (Part I) are summarized as follows:

- We propose a unified framework of the MCR system, with a series of definitions on MCR(n) systems with order n , standard sampling interval (SSI), MCR(n, m) system, and minimum measurable wavelength (MMW).
- Mathematical models are established based on sensor fusion and least square optimization techniques.
- The error theory of the MCR system is presented and the error amplification factor (EAF) is defined to quantify the error accumulation characteristics of MCR systems.
- The stability of the MCR system is defined and propositions are expressed to reveal the basic relationship between MMW and different sparse configurations.
- In particular, the MCR($n, 1$) system is studied, where propositions are put forward to describe the relationship between the EAF and stability of the MCR system.
- The MCR system showed significant advantages over some current techniques for track geometry: for example, gyroscope- and accelerometer-based techniques. It enables us to use low-cost sensors to achieve the same or even higher precision by increasing the number of sensors and amount of sampling frequency. The MCR system can be especially useful for measuring track geometry irregularities with short wavelengths, such as corrugation.

2. Terminologies, variables, and operators

Table 1 describes the terminologies, variables, and operators used in this paper.

3. Unified framework for the MCR system

3.1. MCR system and its derived forms

This paper proposes a series of MCR systems with a unified framework. The measurement principle of an MCR system with order n is illustrated in Fig. 2. A chord formed between two points on the rail, as the straight line \overline{AC} , acts as a reference and the readout of each sensor at the related EP of the chord is the distance (on normal direction) between the EP and rail to be measured. For the convenience of description of MCR systems, definitions to some basic terminologies are given as follows.

Then, the definition of the order of the MCR system is given as

Definition 1: MCR(n) with order n . As illustrated in Fig. 2, an n -order MCR is defined as a chord-based measurement system with all sensors mounted at the EPs of a chord. The i th EP is the point dividing the chord with ratio $i : (n + 1 - i)$.

The sampling interval of a chord reference measurement represents the length of moving step of the chord between two readouts of the sensors mounted on the chord. Particularly, for a given order of the MCR(n) system, the SSI is defined as

Definition 2: SSI of MCR(n). For MCR(n), the SSI is defined as

$$\Delta L_s = \frac{1}{n+1} \cdot L, \quad (1)$$

where L is the length of the reference chord. For a higher order of MCR(n), the SSI, ΔL_s , is smaller (the sampling frequency is higher). Furthermore, in this study high- and low-frequency samplings were considered if the sampling interval was $\Delta L < \Delta L_s$ and $\Delta L > \Delta L_s$, respectively.

Definition 3: MCR(n, m) system. An MCR(n, m) is defined as an n -order MCR system with m sensors mounted at the EPs of a chord. The configuration of the sensor layout (hereafter named as configuration for short) is specified by an increasing sequence $\mathbf{k} = \{k_i | i = 0, 1, \dots, m; k_i \in N^+ \cap [1, n]\}$.

In particular, MCR(n, n), (default MCR(n)) is termed the full configuration of an MCR system with order n , and MCR(n, m), where $m < n$, is a sparse configuration. Among all the sparse configurations, MCR($n, 1$) is known as the conventional three-point chord method [4,5,11–14], and when a single sensor exists at the middle of a chord, the method is called the MCO method [4].

There exist a series of derived MCR systems. Assume that each EP cannot be simultaneously occupied by two sensors, then there are $n!/(m! \cdot (n-m)!)$ configurations for MCR(n, m) systems, e.g., there are 120 configurations for MCR(10, 5).

Definition 4: MMW. The MMW is defined as the minimal wavelength that can be measured by an MCR system. The smaller the MMW, the better is the MCR system.

The ability to measure shorter wavelengths of track irregularity is of great importance in the application of rail measurement because such irregularities, including corrugation, result in a considerable amount of damage to both rail and trains compared to those resulting from long wavelength components. Moreover, the magnitude of short wavelength is smaller and more challenging to measure.

According to the Nyquist–Shannon sampling theorem [30], the following proposition can be given:

Proposition 1.: For an MCR(n) system with full configuration, given the sampling interval $\Delta L \leq \Delta L_s$,

$$\text{MMW} = 2\Delta L_s = \frac{2L}{n+1} \quad (2)$$

Proposition 1 indicates that MMW depends mainly on the order of an MCR system. That is, when the sampling interval is less than the SSI (ΔL_s), MMW of an MCR(n) system equals $2\Delta L_s$. The increasing of sampling frequency will not improve the MMW. The proof of Proposition 1 is given in Appendix A.

3.2. Measurement model

This section discusses the measurement model of the MCR system, and the full configuration of an MCR(n) system with $\Delta L_s = L/(n+1)$. The measurement system MCR(n, m) can be derived accordingly.

Fig. 2(a) shows the macrograph of the measurement of the whole track section. The versine is measured with respect to a reference chord mounted on the rail, where the displacement sensor is fixed at the EP of the chord.

The track section, with length l , is discretized into N segments, each with length ΔL_s . Thus, the number of segments holds the relation $N = l/\Delta L_s$. The track geometry irregularity $f(x)$ to be measured is then discretized into $\mathbf{y} = (y_0, y_1, \dots, y_N)^T$.

Table 1
Terminologies, variables, and operators.

Terminology	Explanation
MCR system	Multipoint Chord Reference System
MCO system	Mid-Chord Offset method
SSI	Standard sampling interval
EP	Equidistance point that divides a chord by equal length segmentations
MMW	Minimum Measurable Wavelength
FTG	False Track Geometry
ith-EP	The <i>i</i> th equidistance point which divides a chord by ratio of <i>i</i> : (<i>n</i> + 1 – <i>i</i>)
FTG	False Track Geometry
EAF	Error Amplification Factor
Variable	Denotation
<i>l, L</i>	length of track section and reference chord, respectively.
<i>n</i>	order of an MCR(<i>n</i>) system.
ΔL_s	= $L/(n + 1)$, Standard Sampling Interval (SSI) of MCR(<i>n</i>) system.
<i>k</i>	= $\{k_i i = 0, 1, \dots, m; k_i \in N^+ \cap [1, n]\}$, an increasing sequence that specifies the configuration of an MCR(<i>n</i>) system.
<i>N</i>	= $(n + 1) \cdot l/L + 1$, the number of discretized segments of a rail section by SSI.
<i>f(x)</i>	continuous description of track geometry to be measured.
y	= $(y_0, y_1, \dots, y_N)^T$. The discretization of <i>f(x)</i> .
y_i	= $(y_i, y_{i+1}, \dots, y_{n+i})^T$, a sample of y covered by the reference chord with length <i>l</i> .
h_i	= $(h_{1,i}, h_{2,i}, \dots, h_{n,i})^T$, the measured chord versine vector relates to y_i .
λ_i	= $i/(n + 1) - 1$, the ratio of the two parts divided by the <i>i</i> th-EP.
$\bar{\lambda}_i$	= $-1 - \lambda_i = -i/(n + 1)$.
λ_k	= $(\lambda_{k_1}, \lambda_{k_2}, \dots, \lambda_{k_m})$.
M	= $[\lambda \mathbf{I} (-1 - \lambda)]$ with $\lambda = (\lambda_1, \lambda_2, \dots, \lambda_n)^T$, the measurement matrix of MCR system.
H	= $[\mathbf{h}_0, \mathbf{h}_1, \dots, \mathbf{h}_{N-n-1}]$, the integrated measured chord versine matrix.
F(y)	= $\mathbf{y}_0, \mathbf{y}_1, \dots, \mathbf{y}_{N-n-1}$, the matrix contains the track geometry to be measured.
H_k, M_k and F_k(y)	assembled with the partial rows of H , M and F(y) with the indexes specified by k .
M_k	= $[\lambda_k \mathbf{I}_k - (1 + \lambda_k)]$.
$\bar{\mathbf{H}}$ and $\bar{\mathbf{H}}_k$	the measured chord versine matrix containing measurement error.
E and E_k	the measurement error matrix.
A_i	$\mathbf{A}_{k_i} = \begin{bmatrix} \lambda_{k_i} & 0 & \dots & 1 & \dots & 0 & \bar{\lambda}_{k_i} \\ \lambda_{k_i} & 0 & \dots & 1 & \dots & 0 & \bar{\lambda}_{k_i} \\ \vdots & \vdots & \ddots & \vdots & \ddots & \vdots & \vdots \\ \lambda_{k_i} & 0 & \dots & 1 & \dots & 0 & \bar{\lambda}_{k_i} \end{bmatrix}$, with each row containing the <i>i</i> th row of M .
$\bar{\mathbf{h}}_i'$	= $\{\bar{h}_{i,0}, \bar{h}_{i,1}, \dots, \bar{h}_{i,N-n-1}\}^T$ is transpose of the <i>i</i> th row of $\bar{\mathbf{H}}$.
$\bar{\mathbf{h}}_{k_i}$	= $(\bar{h}_{k_i,0}, \bar{h}_{k_i,1}, \dots, \bar{h}_{k_i,N-n-1})^T$, is the transpose of the <i>i</i> th row vector of $\bar{\mathbf{H}}_k \mathbf{z}(j)$
U	= $\begin{bmatrix} \mathbf{A}_1 \\ \mathbf{A}_2 \\ \vdots \\ \mathbf{A}_n \end{bmatrix} \cdot \mathbf{y} - \begin{bmatrix} \bar{\mathbf{h}}_1' \\ \bar{\mathbf{h}}_2' \\ \vdots \\ \bar{\mathbf{h}}_n' \end{bmatrix}$, the error vector described by the versine vectors $\bar{\mathbf{h}}_i'$.
U_k	the version of U with sparse configuration.
y*	= $\mathcal{A}_M(\mathbf{H} + \mathbf{E})$, the least square estimation of y .
$\tilde{\mathbf{y}}$	= $\mathbf{y} - \mathbf{y}^* = \mathcal{A}_M(\mathbf{E})$, the False Track Geometry (FTG).
\tilde{y}_p	= $\sum_{i=1}^{n(N-n)} D_{pi} \cdot \text{vec}(\mathbf{E})_i$, the <i>i</i> th value of $\tilde{\mathbf{y}}$.
D	= $[\mathbf{BA}_1^T \quad \mathbf{BA}_2^T \quad \dots \quad \mathbf{BA}_n^T]$.
<i>p</i>	an index refers to position on the rail to be measured.
B	= $(\sum_{i=1}^n \mathbf{A}_i^T \mathbf{A}_i)^{-1}$, if $\sum_{i=1}^n \mathbf{A}_i^T \mathbf{A}_i$ is invertible.
$EAF_p(\mathbf{M}, l)$	= $\sqrt{\sum_{i=1}^{n(N-n)} D_{pi}^2}$, the EAF at location <i>p</i> with given M and length of rail <i>l</i> to be measured.
<i>n_i</i>	= $L_i/\Delta L_s \in N^+$, the occupied shares of the <i>i</i> th segment with respect to SSI ΔL_s .
<i>L_i</i>	the length of the <i>i</i> th segment divided by the sensors with a given configuration k .
<i>d</i>	= $\text{GCD}(n_0, n_1, \dots, n_m)$, the greatest common divisor of n_0, n_1, \dots , and n_m .
<i>n'</i>	= $(n + 1)/d - 1$, the order of a degraded MCR(<i>n</i> , <i>m</i>) systems when $d > 1$.
k'	= k / <i>d</i> , the configuration of a degraded MCR(<i>n</i> , <i>m</i>) systems when $d > 1$.
z(n)	represents a row vector containing <i>n</i> zeros
J_k	a matrix with size of <i>m</i> -by- <i>n</i> with $\mathbf{J}_k(i, j) = \begin{cases} 1, j = k_i \\ 0, j \neq k_i \end{cases}$
Operator	Denotation
<i>E</i> (·)	mathematical expectation of a random variable
<i>Var</i> (·)	variance of a random variable
<i>GCD</i> (·, ·, ·, ·, ·, ·)	greatest common divisor
$\mathcal{A}_M(\mathbf{X})$	= $(\sum_{i=1}^n \mathbf{A}_i^T \mathbf{A}_i)^{-1} \cdot \sum_{i=1}^n \mathbf{A}_i^T (\mathbf{x}_i)$, the restoration operator of MCR system, where \mathbf{x}_i' is transpose of the <i>i</i> th row of matrix X .
<i>ceil</i> (·)	The smallest integer larger than a given real number
X^T	the transpose of X .

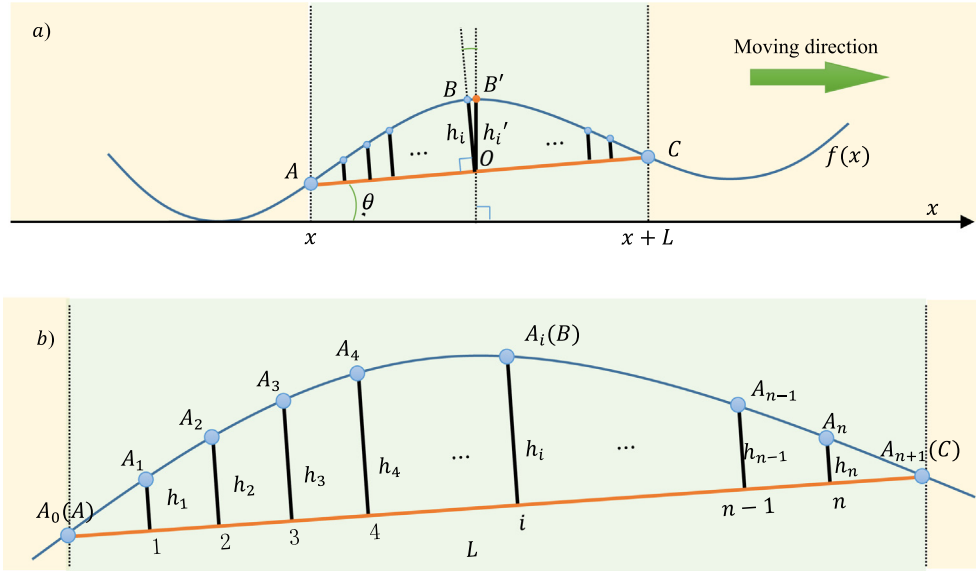


Fig. 2. Measurement principle of the MCR system with order n . Chord length L is divided into $n+1$ equal length segments, and the sensors are mounted at the EPs.

For a given length of the measured chord L , there exists a basic relation between the ratio l/L (the ratio between the lengths of the track section and reference chord) and number of segments N .

$$N = (n + 1) \frac{l}{L} \tag{3}$$

The reference chord moves along the rail, with two ends attached on the rail, as illustrated in Fig. 2(b). At the beginning point, chord length L covers $\mathbf{y}_0 = (y_0, y_1, \dots, y_{n+1})^T$. The n sensors then measure the normal offset from the EP to rail, and we obtain $\mathbf{h}_0 = (h_{1,0}, h_{2,0}, \dots, h_{n,0})^T$. Each $h_{i,0}$ is defines as

$$h_{i,0} = y_i + \lambda_i \cdot y_0 + \bar{\lambda}_i \cdot y_{n+1}; \quad i = 1, 2, \dots, n \tag{4}$$

where λ_i and $\bar{\lambda}_i$ are the ratios

$$\lambda_i = \frac{i}{n+1} - 1 \quad \text{and} \quad \bar{\lambda}_i = -1 - \lambda_i = -\frac{i}{n+1},$$

respectively. Eq. (4) can be written in the matrix form:

$$\mathbf{h}_0 = \mathbf{M} \cdot \mathbf{y}_0 \tag{5}$$

Matrix \mathbf{M} is the essential **measurement matrix** that transforms the target to be measured into measured versine values and is presented as

$$\mathbf{M} = \begin{bmatrix} \lambda_1 & 1 & & \bar{\lambda}_1 \\ \lambda_2 & & 1 & \bar{\lambda}_2 \\ \vdots & & & \vdots \\ \lambda_n & & & 1 & \bar{\lambda}_n \end{bmatrix} \tag{6}$$

The size of \mathbf{M} is $n \times (n+2)$, and it can be rewritten as $\mathbf{M} = [\lambda \mathbf{I} (-1 - \lambda)]$, with $\lambda = (\lambda_1, \lambda_1, \dots, \lambda_n)^T$.

Similarly, when the reference chord moves to location, $\Delta L_s \cdot i$, chord length L covers $\mathbf{y}_i = (y_i, y_{i+1}, \dots, y_{n+i})^T$, the n sensors measure the normal offset from the EP to the rail, and we obtain $\mathbf{h}_i = (h_{1,i}, h_{2,i}, \dots, h_{n,i})^T$. Thus, we get

$$\mathbf{h}_i = \mathbf{M} \cdot \mathbf{y}_i; \quad i = 0, 1, \dots, N - n. \tag{7}$$

The whole measurement process can be integrated as Eq. (8).

$$\mathbf{H} = \mathbf{M} \cdot \mathbf{F}(\mathbf{y}), \tag{8}$$

where

$$\mathbf{F}(\mathbf{y}) = \begin{bmatrix} y_0 & y_1 & & y_{N-n-1} \\ y_1 & y_2 & & y_{N-n} \\ \vdots & \vdots & \dots & \vdots \\ y_{n+1} & y_{n+2} & & y_N \end{bmatrix} \tag{9}$$

$$\mathbf{H} = \begin{bmatrix} h_{1,0} & h_{1,1} & & h_{1,N-n-1} \\ h_{2,0} & h_{2,1} & & h_{2,N-n-1} \\ \vdots & \vdots & \dots & \vdots \\ h_{n,0} & h_{n,1} & & h_{n,N-n-1} \end{bmatrix} \tag{10}$$

Note that when applying an MCR(n) system on a given rail geometry (described as $N+1$ discrete value), we can obtain $n \times (N - n - 1)$ equations. The measurement of \mathbf{y} is unknown beforehand, implying that $\mathbf{F}(\mathbf{y})$ is unknown; however, we can obtain versine matrix \mathbf{H} . Eq. (8) holds the essential relationship between \mathbf{y} and \mathbf{H} . Section 3.3 presents the restoration model that can estimate \mathbf{y} by fusing the versine matrix measured from multiple sensors.

For the MCR(n, m) system with the configuration of $k = \{k_i | i = 0, 1, \dots, m; k_i \in N^+ \cap [1, n]\}$, the measurement equation can be written as

$$\mathbf{H}_k = \mathbf{M}_k \cdot \mathbf{F}(\mathbf{y}), \tag{11}$$

where \mathbf{H}_k and \mathbf{M}_k represent the partial rows of \mathbf{H} and \mathbf{M} , respectively, with the indexes specified by \mathbf{k} .

As the reference chord moves along the rail, the sensors measure the normal offset between the EPs of the chord and rail with a degree of uncertainty, namely, an error term. Considering the error term, Eqs. (8) and (11) can be rewritten as

$$\bar{\mathbf{H}} = \mathbf{H} + \mathbf{E} = \mathbf{M} \cdot \mathbf{F}(\mathbf{y}) + \mathbf{E} \tag{12}$$

$$\bar{\mathbf{H}}_k = \mathbf{H}_k + \mathbf{E}_k = \mathbf{M}_k \cdot \mathbf{F}(\mathbf{y}) + \mathbf{E}_k, \tag{13}$$

where \mathbf{E} is the measurement error of sensor readouts.

$$\mathbf{E} = \begin{bmatrix} e_{1,0} & e_{1,1} & & e_{1,N-n-2} & e_{1,N-n-1} \\ e_{2,0} & e_{2,1} & \dots & e_{2,N-n-2} & e_{2,N-n-1} \\ \vdots & \vdots & \ddots & \vdots & \vdots \\ e_{n-1,0} & e_{n-1,1} & \dots & e_{n-1,N-n-2} & e_{n-1,N-n-1} \\ e_{n,0} & e_{n,1} & & e_{n,N-n-2} & e_{n,N-n-1} \end{bmatrix} \tag{14}$$

3.3. Restoration model

This section presents the restoration model of the MCR(*n*) systems. The restoration process is the reverse of the measurement process.

The restoration model can be described as an optimization model to find the best value of vector **y** to minimize the total error toward the measured versine matrix **H** based on Eq. (8), as expressed in Eq. (15).

$$\min_{\mathbf{y}} \left\| \frac{1}{2} \mathbf{M} \cdot \mathbf{F}(\mathbf{y}) - \bar{\mathbf{H}} \right\|^2 \tag{15}$$

As **F(y)** is an inner-coupled matrix, the optimization model of Eq. (15) is actually a constrained least squares problem. By decoupling **F(y)**, Eq. (15) is transformed into an unconstrained least squares problem, as presented in Eq. (16).

$$\begin{cases} \min E = \frac{1}{2} \mathbf{U}^2 \\ \mathbf{U} = \begin{bmatrix} \mathbf{A}_1 \\ \mathbf{A}_2 \\ \vdots \\ \mathbf{A}_n \end{bmatrix} \cdot \mathbf{y} - \begin{bmatrix} \bar{\mathbf{h}}_1 \\ \bar{\mathbf{h}}_2 \\ \vdots \\ \bar{\mathbf{h}}_n \end{bmatrix} \end{cases}, \tag{16}$$

where $\bar{\mathbf{h}}_i = \{\bar{h}_{i,0}, \bar{h}_{i,1}, \dots, \bar{h}_{i,N-n-1}\}^T$ is the transpose of the *i*th row of $\bar{\mathbf{H}}$, and

$$\mathbf{A}_i = \begin{bmatrix} \lambda_i & 0 & \dots & 1 & \dots & 0 & \bar{\lambda}_i \\ \lambda_i & 0 & \dots & 1 & \dots & 0 & \bar{\lambda}_i \\ \vdots & \vdots & \ddots & \vdots & \ddots & \vdots & \vdots \\ \lambda_i & 0 & \dots & 1 & \dots & 0 & \bar{\lambda}_i \end{bmatrix} \tag{17}$$

where each row of **A_i** contains the *i*th row of **M**. Appendix B proves that Eq. (15) can be equivalent to Eq. (16). The optimal solution of Eq. (16) is equivalent to the linear equation of Eq. (18).

$$\left(\sum_{i=1}^n \mathbf{A}_i^T \mathbf{A}_i \right) \cdot \mathbf{y}^* = \sum_{i=1}^n \mathbf{A}_i^T \bar{\mathbf{h}}_i' \tag{18}$$

When $\sum_{i=1}^n \mathbf{A}_i^T \mathbf{A}_i$ is invertible, the optimal solution of **y*** can be obtained by

$$\mathbf{y}^* = \left(\sum_{i=1}^n \mathbf{A}_i^T \mathbf{A}_i \right)^{-1} \cdot \sum_{i=1}^n \mathbf{A}_i^T \bar{\mathbf{h}}_i' \tag{19}$$

If $\sum_{i=1}^m \mathbf{A}_{k_i}^T \mathbf{A}_{k_i}$ is not invertible, then the Moore–Penrose pseudo-inverse [29] is used.

Similarly, the optimization model for an MCR(*n, m*) system with configuration specified by $k = \{k_i | i = 0, 1, \dots, m; k_i \in N^+ \cap [1, n]\}$ is given as

$$\min_{\mathbf{y}} \left\| \frac{1}{2} \mathbf{M}_k \cdot \mathbf{F}_k(\mathbf{y}) - \bar{\mathbf{H}}_k \right\|^2 \tag{20}$$

Similarly, Eq. (20) can also be equivalent to the following Eqs. (21)–(23):

$$\begin{cases} \min E = \frac{1}{2} \mathbf{U}_k^2 \\ \mathbf{U}_k = \begin{bmatrix} \mathbf{A}_{k_1} \\ \mathbf{A}_{k_2} \\ \vdots \\ \mathbf{A}_{k_m} \end{bmatrix} \cdot \mathbf{y} - \begin{bmatrix} \bar{\mathbf{h}}'_{k_1} \\ \bar{\mathbf{h}}'_{k_2} \\ \vdots \\ \bar{\mathbf{h}}'_{k_m} \end{bmatrix} \end{cases} \tag{21}$$

$$\left(\sum_{i=1}^m \mathbf{A}_{k_i}^T \mathbf{A}_{k_i} \right) \cdot \mathbf{y}^* = \sum_{i=1}^m \mathbf{A}_{k_i}^T \bar{\mathbf{h}}'_{k_i} \tag{22}$$

$$\mathbf{y}^* = \left(\sum_{i=1}^m \mathbf{A}_{k_i}^T \mathbf{A}_{k_i} \right)^{-1} \cdot \sum_{i=1}^m \mathbf{A}_{k_i}^T \bar{\mathbf{h}}'_{k_i} \tag{23}$$

If $\sum_{i=1}^m \mathbf{A}_{k_i}^T \mathbf{A}_{k_i}$ is not invertible, then the Moore–Penrose pseudo-inverse [29] is used.

3.4. Boundary conditions

Another problem concerning the uniqueness of the solution for the estimation of **y*** can be described as the following proposition.

Proposition 2: Given an MCR(*n, m*) system, when no measurement errors are included from sensors, two track geometry sequences **y** and **y*** share the same chord versine matrix **H** if and only if the following condition is satisfied:

$$\mathbf{y} - \mathbf{y}^* = a \cdot \mathbf{x} + b, \tag{24}$$

where **x** is a vector of the position along the rail, and *a* and *b* are the arbitrary real numbers.

The proof of Proposition 2 is given in Appendix A.

Proposition 2 indicates that the measured track geometry may be linear compared to the rail track geometry. To deal with the uniqueness of the solution of the restoration model, additional constrains or boundary conditions are proposed in this paper:

$$y_0 = y_N = 0 \tag{25}$$

Boundary condition Eq. (25) is applied to model Eq. (16) by removing the first and last columns of Eq. (17). The boundary condition Eq. (25) can be understood as using a line with two ends fixed at the beginning and end of the rail as a reference to describe the track geometry to be measured. Actually, the values of *y₀* and *y_N* can be other values, but the final measured result would be equivalent to this double zeros case according to **Proposition 2**. As a result, to make the performance of different MCR systems to be easily compared and interpreted, we use *y₀* = *y_N* = 0 as the default boundary condition thereafter.

4. Error theory of MCR system in the spatial domain

4.1. Error sensitivity of the model

This section presents the analysis of the influence of error term **E** on the restoration performance of measured targets.

First, it should be noted that the measured value $\bar{\mathbf{H}}$ is a linear combination of real versine matrix **H** and error term **E** according to Eq. (12). Define a restoration operator $\mathcal{A}_M(\cdot)$ for a given measurement matrix **M** as

$$\mathcal{A}_M(\mathbf{H}) = \left(\sum_{i=1}^n \mathbf{A}_i^T \mathbf{A}_i \right)^{-1} \cdot \sum_{i=1}^n \mathbf{A}_i^T (\mathbf{h}_i'), \tag{26}$$

where \mathbf{h}_i' is the transpose of the *i*th row of **H** and **A_i** is derived from the *i*th row of measurement matrix **M** according to Eq. (17). If $\sum_{i=1}^m \mathbf{A}_{k_i}^T \mathbf{A}_{k_i}$ is not invertible, the Moore–Penrose pseudo-inverse is used.

$\mathcal{A}_M(\cdot)$ is a linear operator, and by using Eq. (12), we get

$$\mathbf{y}^* = \mathcal{A}_M(\mathbf{H} + \mathbf{E}) = \mathbf{y} + \mathcal{A}_M(\mathbf{E}) = \mathbf{y} + \tilde{\mathbf{y}} \tag{27}$$

This indicates that the restored (measured) track-geometry irregularity is a linear combination of its true value and a false track geometry (FTG) $\tilde{\mathbf{y}}$ induced by error term \mathbf{E} .

This is similar to defining restoration operator $\mathcal{A}_{\mathbf{M}_k}$ with given measurement matrix \mathbf{M}_k for the MCR(n, m) system with the configuration of $\mathbf{k} = \{k_i | i = 0, 1, \dots, m; k_i \in N^+ \cap [1, n]\}$. As a result, the property of operator $\mathcal{A}_{\mathbf{M}(\cdot)}$ (or $\mathcal{A}_{\mathbf{M}_k}$) is key to the performance of MCR systems.

4.2. Eaf

This section proposes an important index to address the error propagation characteristics of $\mathcal{A}_{\mathbf{M}(\cdot)}$. According to Eq. (27), the final measurement error yields $\tilde{\mathbf{y}} = \mathbf{y} - \mathbf{y}^* = \mathcal{A}_{\mathbf{M}}(\mathbf{E})$, indicating that when the measurement error of each sensor, that is, $\mathbf{E} = \mathbf{0}$, is ignored and we get $\tilde{\mathbf{y}} = \mathcal{A}_{\mathbf{M}}(\mathbf{E}) = \mathbf{0}$, the MCR system is absolutely accurate for the measurement task. However, there always exist errors during the measuring process regardless of the sensors used. In practice, the error variance denoted as $\text{Var}(\mathbf{E})$ can range from 1 μm to 0.5 mm. Restoration operator $\mathcal{A}_{\mathbf{M}(\cdot)}$ holds the key to sensor precision $\text{Var}(\mathbf{E})$ and final measurement error $\tilde{\mathbf{y}}$.

$$\mathcal{A}_{\mathbf{M}}(\mathbf{E}) = \left(\sum_{i=1}^n \mathbf{A}_i^T \mathbf{A}_i \right)^{-1} \cdot \sum_{i=1}^n \mathbf{A}_i^T \mathbf{e}_i \tag{28}$$

Matrix \mathbf{B} and vectorization operator $\text{vec}(\cdot)$ are defined as

$$\mathbf{B} \cdot \left(\sum_{i=1}^n \mathbf{A}_i^T \mathbf{A}_i \right) = \mathbf{I}; \text{vec}(\mathbf{X}) = \begin{Bmatrix} \mathbf{x}_1 \\ \mathbf{x}_2 \\ \vdots \\ \mathbf{x}_n \end{Bmatrix}, \tag{29}$$

where \mathbf{I} is an identity matrix and \mathbf{x}_i is the transpose of the i th row of \mathbf{X} .

$$\tilde{\mathbf{y}} = \mathcal{A}_{\mathbf{M}}(\mathbf{E}) = \mathbf{B} \cdot \sum_{i=1}^n \mathbf{A}_i^T \mathbf{e}_i = \left[\mathbf{B}\mathbf{A}_1^T, \mathbf{B}\mathbf{A}_2^T, \dots, \mathbf{B}\mathbf{A}_n^T \right] \cdot \text{vec}(\mathbf{E}) \tag{30}$$

Matrix \mathbf{D} is defined as

$$\mathbf{D} = \left[\mathbf{B}\mathbf{A}_1^T \quad \mathbf{B}\mathbf{A}_2^T \quad \dots \quad \mathbf{B}\mathbf{A}_n^T \right], \tag{31}$$

and we get

$$\tilde{\mathbf{y}} = \mathcal{A}_{\mathbf{M}}(\mathbf{E}) = \mathbf{D} \cdot \text{vec}(\mathbf{E}). \tag{32}$$

Here we notice that $\mathcal{A}_{\mathbf{M}}(\mathbf{E})$ is the product of two parts: matrix \mathbf{D} , depending only on measurement matrix \mathbf{M} and $\text{vec}(\mathbf{E})$, which is the error of sensors.

By observing the p th element of $\tilde{\mathbf{y}}$,

$$\tilde{y}_p = \sum_{i=1}^{n(N-n)} D_{pi} \cdot \text{vec}(\mathbf{E})_i. \tag{33}$$

Error term \mathbf{E} is assumed purely as white noise with zero-mean and variance σ^2 :

$$E(e_i) = 0; E(e_i e_j) = \begin{cases} \sigma^2, & i = j \\ 0, & i \neq j \end{cases}.$$

Furthermore, the evaluation of $E(\tilde{y}_p)$ and $\text{Var}(\tilde{y}_p)$ yields

$$E(\tilde{y}_p) = E \left(\sum_{i=1}^{n(N-n)} D_{pi} \cdot \text{vec}(\mathbf{E})_i \right) = \sum_{i=1}^{n(N-n)} D_{pi} \cdot E(\text{vec}(\mathbf{E})_i) = 0 \tag{34}$$

$$\begin{aligned} \text{Var}(\tilde{y}_p) &= E \left(\left[\tilde{y}_p - E(\tilde{y}_p) \right]^2 \right) = E \left(\left(\sum_{i=1}^{n(N-n)} D_{pi} \cdot \text{vec}(\mathbf{E})_i \right)^2 \right) \\ &= \sigma^2 \cdot \sum_{i=1}^{n(N-n)} D_{pi}^2 \end{aligned} \tag{35}$$

As a result, we define the EAF as

$$\text{EAF}_p(\mathbf{M}, l) = \sqrt{\sum_{i=1}^{n(N-n)} D_{pi}^2} \tag{36}$$

Note that subscript p of $\text{EAF}_p(\mathbf{M}, l)$ indicates the position coordinate along the rail to be measured. \mathbf{M} and l in the bracket indicate that EAF_p only depends on the measurement matrix and length of rail section to be measured. EAF is an important index that can be used to predict the variance of the final measurement error with a given condition of sensor precision, MCR(n, m) system configuration, and length of the section to be measured.

A general EAF for MCR(n, m) is defined as follows:

Definition 5. EAF of the MCR(n, m) system with configuration specified by $\mathbf{k} = \{k_i | i = 0, 1, \dots, m; k_i \in N^+ \cap [1, n]\}$ is defined as

$$\text{EAF}_p(\mathbf{M}_k, l) = \sqrt{\sum_{i=1}^{n(N-n)} D_{pi}^2}, \tag{37}$$

where

$$\mathbf{D} = \left[\mathbf{B}_k \mathbf{A}_{k_1}^T \quad \mathbf{B}_k \mathbf{A}_{k_2}^T \quad \dots \quad \mathbf{B}_k \mathbf{A}_{k_m}^T \right] \tag{38}$$

$$\mathbf{B}_k \cdot \left(\sum_{i=1}^m \mathbf{A}_{k_i}^T \mathbf{A}_{k_i} \right) = \mathbf{I} \tag{39}$$

Moreover, each \mathbf{A}_{k_i} is derived from the i th row of \mathbf{M}_k according to Eq. (17). Subscript p represents the position at $p\Delta L_s$, l is the length of rail section to be measured, and N is the total number of the discretized rail segment, given by Eq. (3).

For given length l of rail section, by using a high-order MCR system with more sensors, the $\text{EAF}_p(\mathbf{M}, l)$ is significantly reduced, indicating that the performance of the MCR system can be enhanced by increasing the order and number of sensors.

4.3. Basic characteristics of EAF

Two typical cases are illustrated in Fig. 3, and Fig. 3(a) shows the EAF of the MCR(20) system with full configuration. The EAF curve is symmetrical with two zero points at the two ends and a maximal point at the middle. This indicates that the accumulation of error is maximized at the middle of the rail section and is minimized when it is close to the two ends. It is because the boundary condition of $y_0 = y_N = 0$ is applied. Notably, different boundary conditions will change the shape of the EAF curve, but as long as the same type of boundary condition is used, the maximal value of EAF can still be used to describe and compare the performance of different MCR systems.

For the MCR(20, 10) system, as the sparse configuration is asymmetrically given as $\mathbf{k} = (1, 2, \dots, 10)^T$, the EAF curve is also asymmetrical but still with two zero points at the two ends. The maximal point does not locate at the middle but is slightly offset to the right. It is an interesting phenomenon, which shows the influence of asymmetrical configuration of MCR(n, m) on the EAF curve.

Moreover, the maximal value of EAF in Fig. 3(a) is less than that of Fig. 3(b), indicating that the performance of the full configura-

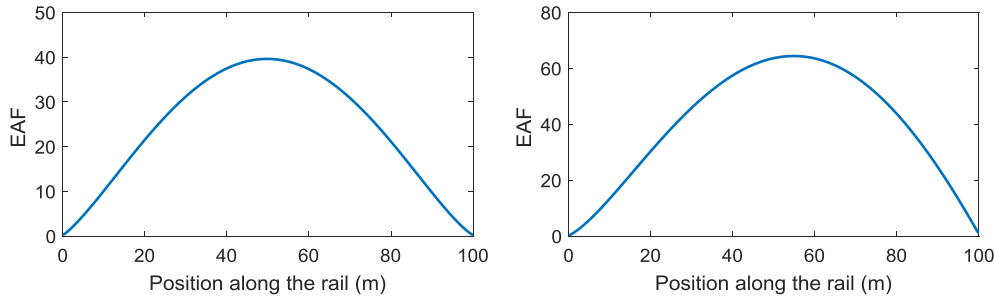


Fig. 3. Illustration of the EAF of (a) the MCR(20) system with full configuration and (b) the MCR(20, 10) system with sparse configuration specified by $\mathbf{k} = (1, 2, \dots, 10)^T$. The maximal EAF of the two systems are 39.6 and 64.4, respectively.

tion is better than that of a sparse configuration under the same order. This is consistent with the fact that full configuration requires more sensors than a sparse configuration.

5. Stability and MMW of MCR systems

5.1. MCR systems with sparse configuration

In application, we always desire to obtain a higher precision with less number of sensors. For MCR(n, m) systems, a higher precision can be achieved by using the so-called *sparse configuration*. We find that we can use less number of sensors but with better layout of the mounting positions or by increasing the order of the MCR system, and we can achieve the same or even higher measurement precision. However, with a more sparse configuration, especially when m is much less than n , the MCR(n, m) system may become *unstable*, and simultaneously, the MMW increases more than $2L/(n + 1)$ with the SSI. This section addresses the issues of the *instability* of the MCR(n, m) system and the degradation of MMW. For this, we provide the condition for the stability of the MCR(n, m) as well as the final MMW.

Before introducing the stability problem, we provide more details on the notations of a sparse configuration with respect to the mounting positions of sensors.

As illustrated in Fig. 4, an MCR(n, m) system is represented by a sparse configuration specified by $\mathbf{k} = \{k_i | i = 0, 1, \dots, m; k_i \in N^+ \cap [1, n]\}$. The m sensors, assuming no overlapping, divide the reference chord into $m+1$ segments. According to **Definition 1**, the k_i th sensor is mounted at the k_i th-EP. The length of the segment between k_i th-EP and k_{i+1} th-EP is denoted as L_i . The relation between n_i and L_i in Fig. 4 is given as

$$n_i = \frac{L_i}{\Delta L_s} \in N^+, \tag{40}$$

where n_i can be understood as the occupied share of the i th segment with respect to SSI ΔL_s . In addition, there exists a basic constraint such that

$$\sum_{i=0}^m L_i = L; \Rightarrow \sum_{i=0}^m n_i = n + 1 \tag{41}$$

Eq. (41) can be defined as m points dividing a line into $m+1$ parts by the sum of each parts and obtaining the total length. For full configuration, that is, $m = n$, we get $n_i = 1$.

5.2. Final MMW of MCR systems with sparse configuration

In general, a smaller sampling interval can achieve higher sampling frequency, and potentially be used to measure shorter wavelengths.

A major benefit of using an MCR system is that it can measure shorter wavelengths, thus achieving a smaller MMW.

However, it is worth noting that by using a higher order MCR systems with *proper configuration*, we can achieve a smaller MMW even with a larger sampling interval, that is, $\Delta L > \Delta L_s$. Here, *proper configuration* implies that for an MCR(n, m) system with a given order n and sensor number m , the configurations play an important role in the MMW, especially when m is considerably smaller than n , namely more sparse configuration.

The MMW depends on not only the order of an MCR(n, m) system but also the specific configuration. The final MMW of an MCR(n, m) system is given by the following proposition.

Proposition 3: Given an MCR(n, m) system with a sparse configuration specified by $\mathbf{k} = \{k_i | i = 0, 1, \dots, m; k_i \in N^+ \cap [1, n]\}$, and given the condition of SSI, $\Delta L_s = L/(n + 1)$,

$$\text{MMW} = 2d\Delta L_s = \frac{2dL}{(n + 1)}, \tag{42}$$

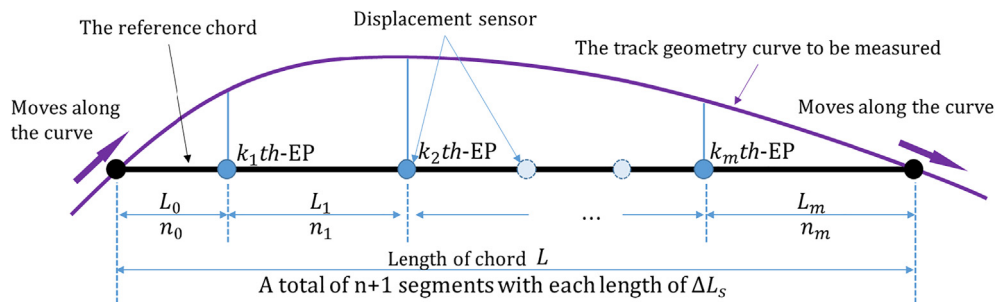


Fig. 4. Illustration of a sparse configuration specified by \mathbf{k} for an MCR(n, m) system.

where $d = \text{GCD}(n_0, n_1, \dots, n_m)$ is the operator for the greatest common divisor of $\{n_i | i = 1, 2, \dots, m\}$. The proof of Proposition 3 is given in Appendix A.

5.3. Stability of MCR systems

Based on **Proposition 3**, the stability of an MCR system is defined as

Definition 6. An $\text{MCR}(n, m)$ system is defined as **stable** if $\text{MMW} = 2\Delta L_s$ with sampling interval $\Delta L \leq \Delta L_s$, and **unstable** otherwise.

The condition for an $\text{MCR}(n, m)$ system to be **unstable** is given as follows:

Proposition 4. Given an $\text{MCR}(n, m)$ system with a sparse configuration specified by $\mathbf{k} = \{k_i | i = 0, 1, \dots, m; k_i \in \mathbb{N}^+ \cap [1, n]\}$, the $\text{MCR}(n, m)$ system is **unstable** if it meets the following condition

- A. $d = \text{GCD}(n_0, n_1, \dots, n_m) > 1$
- B. The given $\text{MCR}(n, m)$ is equivalent to d -degraded $\text{MCR}(n', m)$ systems with $n' = (n + 1)/d - 1$ and configuration specified by $\mathbf{k}' = \mathbf{k}/d$.

where $\text{GCD}(n_0, n_1, \dots, n_m)$ refers to the greatest common divisor of n_0, n_1, \dots, n_m . In fact, conditions A and B in Proposition 4 are equivalent. The proof of Proposition 4 is given in Appendix A.

6. MCR(n, 1) system

6.1. Stability

This section presents the analysis of the stability of the $\text{MCR}(n, 1)$ system with respect to different orders and configurations.

The $\text{MCR}(n, 1)$ system refers to a series of n -order MCR systems with the most sparse configuration, which contains only one sen-

sor on the reference chord; thus, the $\text{MCR}(n, 1)$ system can be more delicate compared to $\text{MCR}(n, m)$ systems with $m > 1$. As mentioned in Section 3.1, $\text{MCR}(n, 1)$ is known as the conventional three-point chord method [4,5,11–14], and when the single sensor is at the middle of a chord, the system is called an MCO method [4,11–13]. Note that by using the unified framework proposed in Section 3, this study dealt with the measurement and restoration processes in a relatively different manner.

An $\text{MCR}(n, 1)$ system possesses $\text{ceil}((n + 1)/2)$ different configurations when considering symmetric distribution, e.g., configurations of $k = 1$ and $k = n$ are symmetric to each other. Figs. 5–7 illustrate the performance of an $\text{MCR}(n, 1)$ system considering different configurations based on numerical analysis. The black curve in the figure represents a target track geometry from track inspection car. The measurement process is simulated according to Eq. (8), following the restoration process based on the equations given in Section 3.3.

Fig. 5 shows six configurations of the performance of $\text{MCR}(11, 1)$ systems. Apparently, the configurations with $k = 2, 3, 4,$ and 6 are unstable. Furthermore, Fig. 6 enlarges the right-bottom figure of Fig. 5. The red dotted line (similar with red shade) represents the original result of $\text{MCR}(11, 1)$. The figure shows that the measured result is a mixture of the six curves of the degraded $\text{MCR}(1, 1)$ systems, and the data points seem to jump up and down, as represented by the red-shaded region.

Fig. 7 shows six configurations of $\text{MCR}(12, 1)$ system performance. In contrast to those in Fig. 5, all six configurations show a stable pattern. The difference between the performances of the two examples can be explained by the following proposition.

Proposition 5. An $\text{MCR}(n, 1)$ system is **stable** for all configurations $\forall k \in \{1, 2, \dots, n\}$ if and only if $n + 1$ is a prime number.

The proof of Proposition 5 is given in Appendix A.

6.2. Eaf

This section presents the analysis of the stability of the $\text{MCR}(n, 1)$ system, and two cases are discussed to illustrate the relation

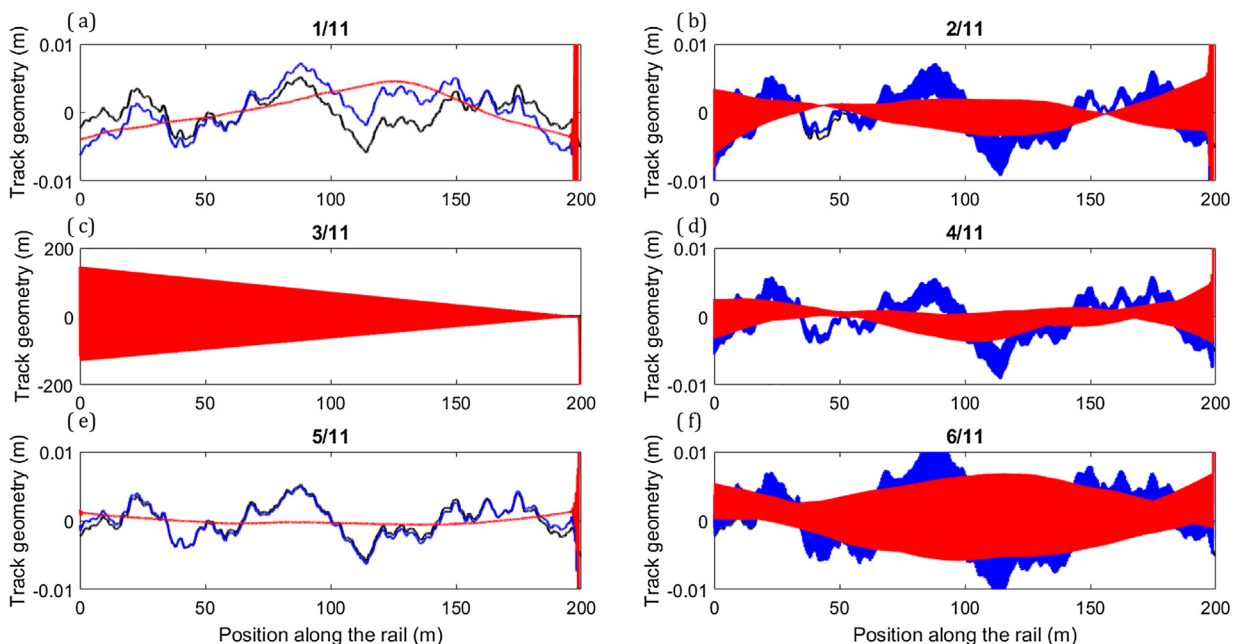


Fig. 5. Configurations of $\text{MCR}(11, 1)$ system performance. The black curves represent the measurement target, namely the track-geometry irregularity sample. The blue curves represent the measured result, considering $2 \mu\text{m}$ sensor uncertainty. The red curves represent the difference between the measurement target and measured result.

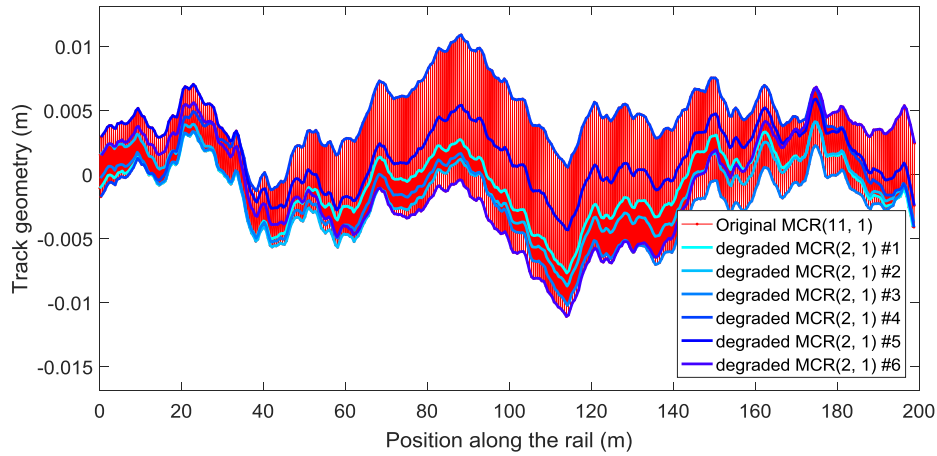


Fig. 6. Degradation of MCR(11, 1) systems with configuration specified by $k = 6$. The red dotted line (similar to the red shaded region) is the original result of MCR(11, 1), which is the same as the Fig. 5(f).

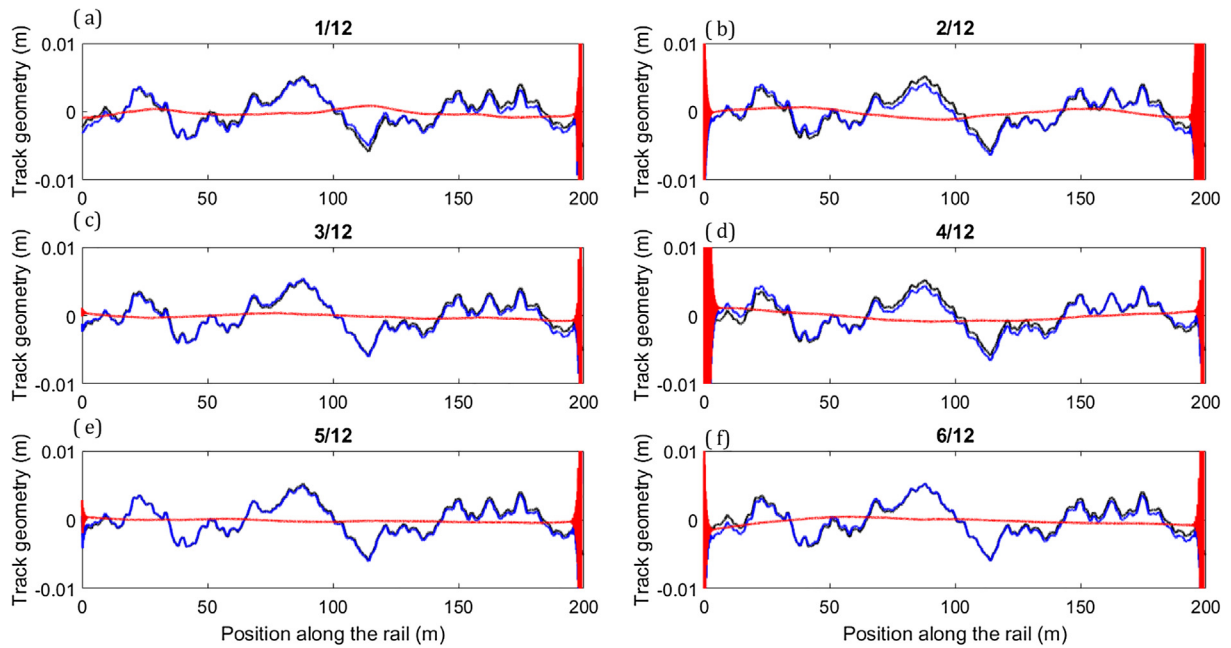


Fig. 7. Six configurations of MCR(12, 1) system performance. Each configuration witnesses a stable pattern, and an edge error can be observed.

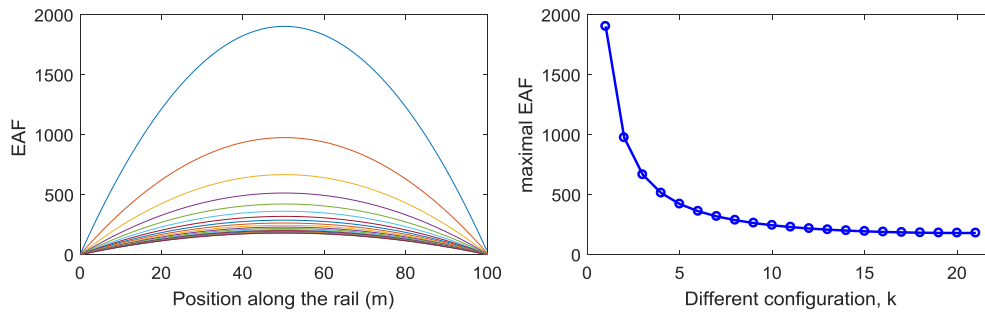


Fig. 8. EAFs of MCR(40, 1) systems with respect to different configurations.

between an unstable $MCR(n, 1)$ system and its degraded $MCR(n', 1)$ system. The EAF was used to reveal the different characteristics between the stable and unstable $MCR(n, 1)$ systems.

First, the EAFs of the three groups of $MCR(n, 1)$ systems were calculated according to Eq. (37), as illustrated in Figs. 8–10. Fig. 8 shows the $MCR(40, 1)$ systems with configurations of $k = 1, 2, \dots$

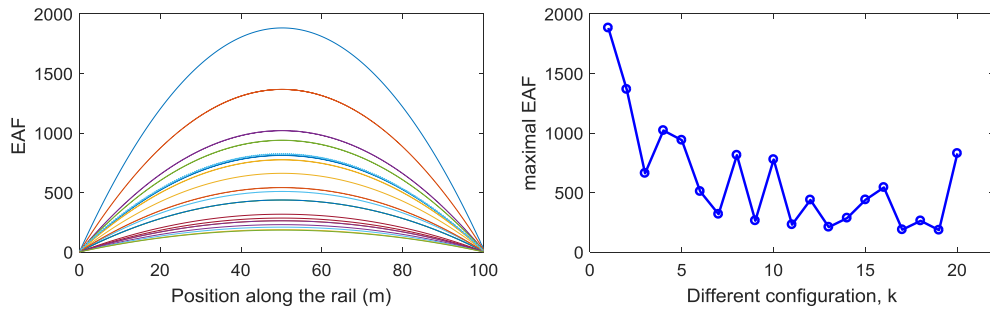


Fig. 9. EAFs of MCR(39, 1) systems with respect to different configurations. When $k = 4, 5, 8, 10, 12, 14, 15, 16, 18,$ and 20 , the maximal EAFs show an unusual increasing trend, and these configurations are all unstable according to Proposition 3.

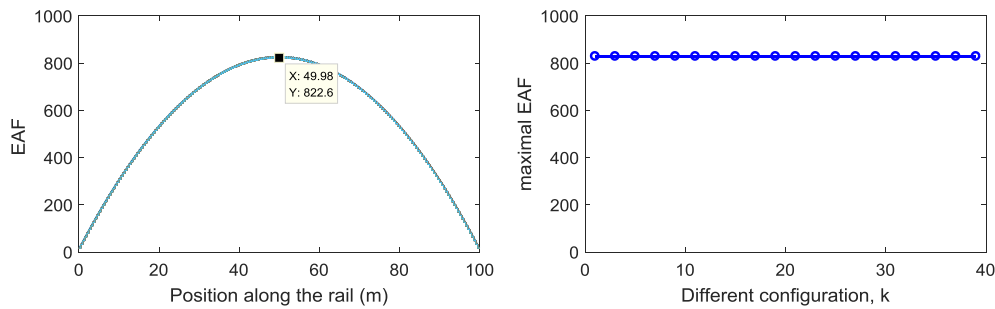


Fig. 10. EAFs of MCR($n, 1$) systems of order $n = 1, 3, \dots, 39$, with the configuration $k = (n + 1)/2 = 1, 2, \dots, 20$, respectively.

20. The maximal EAFs show a monotonously decreasing trend with the increase of configuration number k up to 20. Fig. 9 shows that for MCR(39, 1) systems, when $k = 4, 5, 8, 10, 12, 14, 15, 16, 18,$ and 20 , the maximal EAFs shows an unusual increasing trend; these configurations are all *unstable* according to Proposition 4. Fig. 10 shows a series of MCR($n, 1$) systems for order $n = 1, 3, \dots, 39$ with configuration $k = (n + 1)/2 = 1, 2, \dots, 20$, respectively. The maximal EAFs are almost identical to each other and the value is approximately 822.6. Recalling from our previous publication [4], the EAF of the MCO-systems under the same condition (1 m length chord to measure a 100 m rail) is just the same value.

Based on the above-mentioned three cases, we can draw the following conclusion (Proposition 6).

Proposition 6: Given an **unstable** MCR(n, m) system with configuration specified by $k = \{k_i | i = 0, 1, \dots, m; k_i \in N^+ \cap [1, n]\}$ and $d = \text{GCD}(n_0, n_1, \dots, n_m) > 1$, then the EAF of this MCR(n, m) equals to the EAF of the degraded MCR(n', m) system, where $n' = (n + 1)/d - 1$ and configuration $k' = k/d$.

The proof of Proposition 6 is given in Appendix A.

7. Discussion

This paper does not aim at proposing a single measurement technique but introducing a whole MCR framework with a series of MCR systems as well as the tools to quantify and compare the performance of different configurations. Several definitions and propositions are given to present the basic theory for the measurement principle of MCR systems. However, it is still not enough for fully understanding MCR systems. The following points have not been covered by this paper and are a topic of interest for future study.

- EAF quantifies the error accumulation characteristics of MCR systems with different orders and configurations in the spatial domain. The measurement performance in *frequency domain* (or wavelength domain) remains unclear.
- The performances of *high-* and *low-frequency sampling* compared to that of standard sampling are of interest as they provide an additional parameter to control the measurement precision by increasing or decreasing the sampling frequency. This could offer a trade-off between measurement precision and hardware cost.
- Sections 4.3 and 6.2 show that the sparse configuration is of essential importance to the performance of an MCR system. This raises new queries: what is the best configuration of a MCR(n, m) system? Can we achieve higher precision with smaller number of sensors? What could be the limitation in precision of an MCR(n, m) system? This results in an *optimization* problem with respect to the many sparse configurations.

Note that the measurement chord is always divided into an integer number of segments with a given order of an MCR system. Actually, there exist several configurations in which a sensor can be mounted at a point dividing a chord by a ratio, which is an irrational number. These kinds of configurations are beyond the framework of the MCR system proposed in this paper. Nevertheless, the impracticality of the configurations with precisely irrational ratio divisions is immaterial because even the installation error of the measurement equipment may be much larger than the accuracy of an irrational number with several digits after the decimal point.

The significant advantages of the MCR system over some currently used techniques for track geometry, such as the single-point chord method [4,5,11–14], gyroscope-based techniques [31], and accelerometer-based techniques [32] are summarized as follows.

- The MCR system enables us to use low-cost sensors to achieve the same or even higher precision by increasing the number sensors and sampling frequency.
- We can achieve better precision by adding sensors and improving the configurations without significantly increasing the hardware cost. In contrast, for techniques such as gyroscope-based techniques, adding an additional gyroscope may double the cost and the precision may not be enhanced significantly.
- The MCR system can measure smaller MMW; this is the most powerful advantage over many current techniques. The high-order MCR(n, m) systems are particularly useful for measuring rail corrugations, whose wavelengths may even reach several millimeters.

8. Conclusion

A unified framework of MCR systems is introduced with definitions of n -ordered MCR(n) systems, SSI, MCR(n, m) system, and MMW.

Mathematical models were established to describe the measurement and restoration processes as well as some necessary boundary conditions. The error theory of an MCR system is provided in Section 4 and the EAF is defined to quantify the error accumulation characteristics of MCR systems.

In addition to the error theory, Section 5 introduces another important characteristic about the stability and MMW of MCR systems. The stability of MCR system is defined and propositions are given to reveal the basic relationship between MMW and different sparse configurations.

Section 6 discusses the MCR($n, 1$) system in particular, for which Proposition 6 was put forward to describe the relationship between the EAF and MCR system stability.

Although the MCR system in this paper is focused on the field of railway engineering, it can be applied to any similar application scenarios where an irregular surface or curve needs to be measured. The numerical and experimental verification of MCR systems is considerably challenging and requires considerable amount of effort. This will be addressed in our further works.

Acknowledgements

The present work has been supported by the National Natural Science Foundation of China (51425804, 51608459, and 51378439) and the United Fund for Key Projects of China’s High-Speed Railway (U1334203 and U1234201). The authors Yuan Wang (No. 201707000036) and Huiyue Tang (No. 201707000037) are financially supported by the China Scholarship Council CSC. Dr. Xiang Liu is funded by the US Federal Railroad Administration at the time of writing this paper. However, the authors are solely responsible for all views and analyses in this research.

Appendix A: Proof of Proposition 1–6

Proposition 1: For an MCR(n) system with full configuration, given the sampling interval $\Delta L \leq \Delta L_s$,

$$MMW = 2\Delta L_s = \frac{2L}{n+1} \tag{2}$$

Proof of Proposition 1:

First, according to the Nyquist–Shannon sampling theorem [30], a perfect reconstruction of a signal is guaranteed possible for band-limit $B < F_s/2$ for given sample rate F_s . Here, for an MCR(n) system with full configuration, given $\Delta L = \Delta L_s$ (here, $F_s = 1/\Delta L = 1/\Delta L_s$), the reconstructed track geometry curve is guaranteed possible for band-limit $B < F_s/2 = 1/(2\Delta L_s)$. In wavelength domain, according to the definition 4, we get

$$MMW = \min\left(\frac{1}{B}\right) = 2\Delta L_s \tag{A1}$$

The use of definition 2 (Eq. (1)) yields

$$MMW = 2\Delta L_s = \frac{2L}{n+1}.$$

The remainder of the problem is to prove that improving sample rate F_s (decreasing the sampling interval for $\Delta L < \Delta L_s$) will not result in a larger band-limit B (or will not decrease MMW) (See Fig. A1).

For sampling interval $\Delta L = \Delta L_s$, through the measurement process using an MCR system, we obtain an SSI of $\mathbf{y}_s = (y_0, y_1, \dots, y_N, \dots)^T$. For sequence \mathbf{y}_s , we can achieve $MMW = 2\Delta L_s = 2L/(n+1)$.

Given a sampling interval $\Delta L = \Delta L_s/\tau$, where $\tau > 1$, the measurement process using the MCR system yields a sampling sequence that is τ times the number of \mathbf{y}_s , denoted as $\mathbf{y}_\tau = (y_0, y_1, \dots, y_\tau, y_{\tau+1}, \dots, \dots, y_{N\tau}, y_{N\tau+1}, \dots)^T$.

Furthermore, when τ is an integer, as illustrated in Fig. A1, sequence \mathbf{y}_τ can be changed into τ independent sequences

$$\{\mathbf{y}_{\tau,i} | i = 0, 1, \dots, \tau - 1; \mathbf{y}_{\tau,i} = (y_i, y_{\tau+i}, \dots, y_{N\tau+i}, \dots)^T\} \tag{A2}$$

This implies that each $\mathbf{y}_{\tau,i}$ is independently measured without any connection. We know that the measurement of $\mathbf{y}_{\tau,i}$ is equivalent to an MCR system with a SSI but with different starting points. That is, \mathbf{y}_τ is actually equivalent to τ independent measurements with $\Delta L = \Delta L_s$ with different starting points. As a result, this kind of τ -times repeated measurement can improve the measurement precision but will not improve MMW.

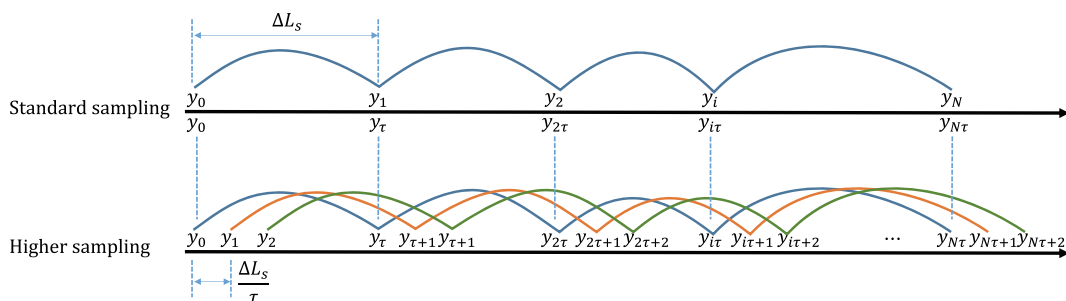


Fig. A1. The upper figure illustrates a standard sampling with $\Delta L = \Delta L_s$, and the lower figure illustrates that for $\Delta L = \Delta L_s/\tau$, where $\tau > 1$ is an integer. Different colors indicate measurement sequence with different starting points.

When τ is not an integer, \mathbf{y}_τ can be transformed into a sequence with an integer multiple number of \mathbf{y}_s through interpolation. Note that the interpolation will not improve the MMW as it brings no additional information, instead it only changes the formation of sequence \mathbf{y}_τ .

Proposition 2.: Given an MCR(n, m) system, when no measurement errors from sensors are included, two track geometry sequences \mathbf{y} and \mathbf{y}^* share the same chord versine matrix \mathbf{H} if and only if the following condition is satisfied.

$$\mathbf{y} - \mathbf{y}^* = a \cdot \mathbf{x} + b, \tag{24}$$

where \mathbf{x} is a vector of the position along the rail and a and b are the arbitrary real numbers.

Proof of Proposition 2:

Proof of sufficiency: Assuming that sequences \mathbf{y} and \mathbf{y}^* share chord versine matrix \mathbf{H} , prove that $\mathbf{y} - \mathbf{y}^*$ can be expressed as the form of $a \cdot \mathbf{x} + b$.

According to the given condition and by using Eq. (8), we get

$$\mathbf{H} = \mathbf{M} \cdot \mathbf{F}(\mathbf{y}) = \mathbf{M} \cdot \mathbf{F}(\mathbf{y}^*) \tag{A3}$$

According to Eq. (9), $\mathbf{F}(\mathbf{y})$ is a matrix generated by a given sequence \mathbf{y} and is a linear operator; thus, we get

$$\mathbf{M} \cdot \mathbf{F}(\mathbf{y}) - \mathbf{M} \cdot \mathbf{F}(\mathbf{y}^*) = \mathbf{M} \cdot \mathbf{F}(\mathbf{y} - \mathbf{y}^*) = 0 \tag{A4}$$

Based on the definition of λ_i , $\mathbf{M} \cdot \mathbf{F}(\mathbf{x}) = 0$ is satisfied when \mathbf{x} is a linear function. As a result, there exist coefficients a and b such that

$$\mathbf{y} - \mathbf{y}^* = a \cdot \mathbf{x} + b,$$

$$\mathbf{x} = (1, 2, \dots, N)^T$$

Proof of necessity: Given $\mathbf{y}^* = \mathbf{y} + a \cdot \mathbf{x} + b$ and the corresponding chord versine matrix of \mathbf{y} is \mathbf{H} , prove that \mathbf{H} is also the chord versine matrix of \mathbf{y}^* .

According to the given condition and by using Eq. (8), we get

$$\begin{aligned} \mathbf{H} &= \mathbf{M} \cdot \mathbf{F}(\mathbf{y}) = \mathbf{M} \cdot \mathbf{F}(\mathbf{y}^* - a \cdot \mathbf{x} - b) \\ &= \mathbf{M} \cdot \mathbf{F}(\mathbf{y}^*) - \mathbf{M} \cdot \mathbf{F}(a \cdot \mathbf{x} + b) \end{aligned} \tag{A5}$$

Based on the definition of λ_i and by using Eq. (4), we get

$$\mathbf{M} \cdot \mathbf{F}(a \cdot \mathbf{x} + b) = 0, \tag{A6}$$

and then

$$\mathbf{M} \cdot \mathbf{F}(\mathbf{y}^*) = \mathbf{H}$$

Thus, Proposition 2 is proved.

Proposition 3.: Given an MCR(n, m) system with a sparse configuration specified by $\mathbf{k} = \{k_i | i = 0, 1, \dots, m; k_i \in N^+ \cap [1, n]\}$ and given the condition of SSI, $\Delta L_s = L / (n + 1)$,

$$\text{MMW} = 2d\Delta L_s = \frac{2dL}{(n + 1)}, \tag{42}$$

where $d = \text{GCD}(n_0, n_1, \dots, n_m)$ is an operator for greatest common divisor of $\{n_i | i = 1, 2, \dots, m\}$.

Proof of Proposition 3:

The condition of $d = \text{GCD}(n_0, n_1, \dots, n_m) = 1$ can be proved similarly by using **Proposition 1**. Then, we should only focus on the cognition of $d > 1$.

First, the measurement matrix \mathbf{M}_k of MCR (n, m) system with sparse configuration specified by \mathbf{k} is given by partial rows of \mathbf{M} with the indexes specified by \mathbf{k} .

$$\mathbf{M}_k = [\lambda_k \quad \mathbf{J}_k \quad -(1 + \lambda_k)], \tag{A7}$$

where $\lambda_k = (\lambda_{k_1}, \lambda_{k_2}, \dots, \lambda_{k_m})$, and \mathbf{J}_k is a matrix with size of $m \times n$, as

$$\mathbf{J}_k(i, j) = \begin{cases} 1, j = k_i \\ 0, j \neq k_i \end{cases}; i = 1, \dots, m; j = 1, \dots, n \tag{A8}$$

By expanding Eq. (11), we get

$$\begin{aligned} &[\lambda_k \quad \mathbf{J}_k \quad -(1 + \lambda_k)] \cdot \begin{bmatrix} y_0 & y_1 & \dots & y_{N-n-1} \\ y_1 & y_2 & \dots & y_{N-n} \\ \vdots & \vdots & \dots & \vdots \\ y_{n+1} & y_{n+2} & \dots & y_N \end{bmatrix} \\ &= \begin{bmatrix} h_{k_1,0} & \dots & h_{k_1,N-n-1} \\ h_{k_2,0} & \dots & h_{k_2,N-n-1} \\ \vdots & \ddots & \vdots \\ h_{k_m,0} & \dots & h_{k_m,N-n-1} \end{bmatrix} \end{aligned} \tag{A9}$$

The above equation is equivalent to

$$\begin{aligned} &[\lambda_k \quad \mathbf{I}_m \quad -(1 + \lambda_k)] \cdot \begin{bmatrix} y_0 & y_1 & \dots & y_{N-n-1} \\ y_{k_1} & y_{k_1+1} & \dots & y_{k_1+N-n-1} \\ \vdots & \vdots & \dots & \vdots \\ y_{k_m} & y_{k_m+1} & \dots & y_{k_m+N-n-1} \\ y_{n+1} & y_{n+2} & \dots & y_N \end{bmatrix} \\ &= \begin{bmatrix} h_{k_1,0} & \dots & h_{k_1,N-n-1} \\ h_{k_2,0} & \dots & h_{k_2,N-n-1} \\ \vdots & \ddots & \vdots \\ h_{k_m,0} & \dots & h_{k_m,N-n-1} \end{bmatrix} \end{aligned} \tag{A10}$$

where \mathbf{I}_m is an identity matrix with size m .

With the given integer $d > 1$, the above equation can be separated into d parts:

$$\begin{aligned} &[\lambda_k \quad \mathbf{I}_k \quad -(1 + \lambda_k)] \cdot \begin{bmatrix} y_i & y_{d+i} & \dots & y_{Td+i} \\ y_{k_1+i} & y_{k_1+d+i} & \dots & y_{k_1+Td+i} \\ \vdots & \vdots & \dots & \vdots \\ y_{k_m+i} & y_{k_m+d+i} & \dots & y_{k_m+Td+i} \\ y_{n+i} & y_{n+d+i} & \dots & y_{n+Td+i} \end{bmatrix} \\ &= \begin{bmatrix} h_{k_1,i} & \dots & h_{k_1,Td+i} \\ h_{k_2,i} & \dots & h_{k_2,Td+i} \\ \vdots & \ddots & \vdots \\ h_{k_m,i} & \dots & h_{k_m,Td+i} \end{bmatrix}, i = 0, \dots, d - 1 \end{aligned} \tag{A11}$$

where T is an integer satisfying

$$n + Td + d - 1 = N \tag{A12}$$

Simple notations \mathbf{M}_k^* , $\mathbf{F}_i(\mathbf{y})$, and \mathbf{H}_i are introduced as

$$\mathbf{M}_k^* = [\lambda_k \quad \mathbf{I}_k \quad -(1 + \lambda_k)] \tag{A13}$$

$$\mathbf{F}_i(\mathbf{y}) = \begin{bmatrix} y_i & y_{d+i} & \dots & y_{Td+i} \\ y_{k_1+i} & y_{k_1+d+i} & \dots & y_{k_1+Td+i} \\ \vdots & \vdots & \dots & \vdots \\ y_{k_m+i} & y_{k_m+d+i} & \dots & y_{k_m+Td+i} \\ y_{n+i} & y_{n+d+i} & \dots & y_{n+Td+i} \end{bmatrix}; i = 0, \dots, d - 1 \tag{A14}$$

$$\mathbf{H}_i = \begin{bmatrix} h_{k_1,i} & \dots & h_{k_1,Td+i} \\ h_{k_2,i} & \dots & h_{k_2,Td+i} \\ \vdots & \ddots & \vdots \\ h_{k_m,i} & \dots & h_{k_m,Td+i} \end{bmatrix}; i = 0, \dots, d - 1 \tag{A15}$$

We get

$$\mathbf{M}_k^* \cdot \mathbf{F}_i(\mathbf{y}) = \mathbf{H}_i; i = 0, \dots, d - 1 \quad (\text{A16})$$

Denote d number of sets, $\mathbf{S}_i, i = 0, \dots, d - 1$, each containing all the elements inside $\mathbf{F}_i(\mathbf{y})$. By using condition $d = \text{GCD}(n_0, n_1, \dots, n_m) > 1$, we found that the d equations $(\mathbf{M}_k^* \cdot \mathbf{F}_i(\mathbf{y}) = \mathbf{H}_i; i = 0, \dots, d - 1)$ are independent as the intersection of any two sets from $\{\mathbf{S}_i | i = 0, 1, \dots, d - 1\}$ is an empty set.

Considering that each \mathbf{S}_i is also an equidistant sampling sequence from \mathbf{y} , it can be treated as a new measurement by the degraded MCR(n', m) system with a sampling interval of $\Delta L_s \cdot d$. The order of an MCR system becomes $n' = (n + 1)/d - 1$ and the configuration is specified by an increasing sequence of $k' = k/d$.

As a result, the MMW is given by

$$\text{MMW} = 2d\Delta L_s = \frac{2dL}{(n + 1)} \quad (\text{A2})$$

Thus, we proved Proposition 3.

Proposition 4. Given an MCR(n, m) system with a sparse configuration specified by $k = \{k_i | i = 0, 1, \dots, m; k_i \in N^+ \cap [1, n]\}$, the MCR(n, m) system is unstable if it meets the following condition

- C. $d = \text{GCD}(n_0, n_1, \dots, n_m) > 1$
- D. The given MCR(n, m) is equivalent to d degraded MCR(n', m) systems with $n' = (n + 1)/d - 1$ and configuration specified by $k' = k/d$.

Proposition 4 can be proved using **Proposition 3** and **Definition 6**. To avoid repetition, it is not described here.

Proposition 5. An MCR($n, 1$) system is stable for all configurations $\forall k \in \{1, 2, \dots, n\}$ if and only if $n + 1$ is a prime number.

Proof of Proposition 5:

Proof of sufficiency. We used reduction to absurdity to prove it. Assuming $n + 1$ is not a prime number and the MCR($n, 1$) system is still stable for all configurations $\forall k \in \{1, 2, \dots, n\}$. As $n + 1$ is not a prime number, we can find two integers $a > 1$ and $b > 1$ satisfying

$$n + 1 = a \cdot b. \quad (\text{A17})$$

As a is an integer greater than 1, we can find two positive integers b_1 and b_2 satisfying

$$n + 1 = a \cdot b = a \cdot (b_1 + b_2). \quad (\text{A18})$$

Then, construct an MCR($n, 1$) system with configuration given by $k = a \cdot b_1$, which divides a reference chord in two with shares of $a \cdot b_1$ and $a \cdot b_2$.

Finally, $d = \text{GCD}(a \cdot b_1, a \cdot b_2) \geq a > 1$, which conflicts with **Proposition 4**.

Proof of necessity. Again, we use reduction to absurdity to prove it. Assume that $n + 1$ is a prime number and there exists configuration k for MCR($n, 1$) system, which is unstable. Denote the two shares of chord divided by k as n_0 and n_1 satisfying

$$n + 1 = n_0 + n_1 \quad (\text{A19})$$

As the MCR($n, 1$) system is unstable, we get

$$d = \text{GCD}(n_0, n_1) > 1 \quad (\text{A20})$$

This implies that we can find two integers $a > 1$ and $b > 1$ satisfying $n_0 = d \cdot a$ and $n_1 = d \cdot b$, respectively, thus yielding

$$n + 1 = n_0 + n_1 = d \cdot a + d \cdot b = d \cdot (a + b) \quad (\text{A21})$$

This conflicts with the assumption that $n + 1$ is a prime number as d and $a + b$ are both factors of $n + 1$ and are > 1 .

Thus, we proved Proposition 5.

Proposition 6. Given an unstable MCR(n, m) system with configuration specified by $k = \{k_i | i = 0, 1, \dots, m; k_i \in N^+ \cap [1, n]\}$ and $d = \text{GCD}(n_0, n_1, \dots, n_m) > 1$, then the EAF of this MCR(n, m) equals the EAF of the degraded MCR(n', m) system, where $n' = (n + 1)/d - 1$ and configuration $k' = k/d$.

Proof of Proposition 6:

Note: The variables with the ' symbol represent variables for a degraded MCR system with respect to the original MCR system.

According to **Proposition 4**, when $d = \text{GCD}(n_0, n_1) > 1$, the MCR(n, m) system is unstable and degrades to MCR(n', m) with $n' = (n + 1)/d - 1$ and configuration specified by $k' = k/d$. By observing and comparing the sparse structures of \mathbf{A}_{k_i} and $\mathbf{A}_{k'_i}$ according to Eq. (17), we obtain the following relationship:

$$\mathbf{A}_{k_i}(l, j) = \begin{cases} 0, & \text{mod}(j, d) \neq 1 \\ \mathbf{A}_{k'_i}\left(\frac{l-1}{d}, \frac{j-1}{d}\right), & \text{mod}(j, d) = 1; \forall l \in [1, N - n] \end{cases} \quad (\text{A22})$$

where $\mathbf{A}_{k_i}(l, j)$ in Eq. (A21) represents the l th row vector of \mathbf{A}_{k_i} beginning from the l th column to the end of the l th row (This is the same for $\mathbf{A}_{k'_i}$).

Define matrixes \mathbf{A}_k and $\mathbf{A}_{k'}$ as

$$\mathbf{A}_k = \sum_{i=1}^m \mathbf{A}_{k_i}^T \mathbf{A}_{k_i}; \quad \mathbf{A}_{k'} = \sum_{i=1}^m \mathbf{A}_{k'_i}^T \mathbf{A}_{k'_i} \quad (\text{A23})$$

Structures \mathbf{A}_k and $\mathbf{A}_{k'}$ show that

$$\mathbf{A}_k(i, j) = \begin{cases} 0, & \text{mod}(i, d) \neq 1 \text{ or } \text{mod}(j, d) \neq 1 \\ \mathbf{A}_{k'}\left(\frac{i-1}{d}, \frac{j-1}{d}\right), & \text{mod}(i, d) = 1 \text{ and } \text{mod}(j, d) = 1 \end{cases} \quad (\text{A24})$$

where $\mathbf{A}_k(i, j)$ represents the element at i th row and j th column of \mathbf{A}_k (similarly for $\mathbf{A}_{k'}$). Moreover, Eq. (39) can be used to verify that

$$\mathbf{B}_k(i, j) = \begin{cases} 0, & \text{mod}(i, d) \neq 1 \text{ or } \text{mod}(j, d) \neq 1 \\ \mathbf{B}_{k'}\left(\frac{i-1}{d}, \frac{j-1}{d}\right), & \text{mod}(i, d) = 1 \text{ and } \text{mod}(j, d) = 1 \end{cases} \quad (\text{A25})$$

Recalling the definition of EAF (**Definition 5**) given by Eq. (37) and by using Eq. (38), $\text{EAF}_p(\mathbf{M}_k, l)^2$ can be rewritten as

$$\text{EAF}_p(\mathbf{M}_k, l)^2 = \sum_{i=1}^{m(N-n)} D_{pi}^2 = \sum_{i=1}^m \sum_{j=1}^{N-n} (\mathbf{B}_{k,p}^T \cdot \mathbf{A}_{k_i,j})^2, \quad (\text{A26})$$

where $\mathbf{B}_{k,p}^T$ denotes the transpose of the p th column vector of \mathbf{B}_k and $\mathbf{A}_{k_i,j}$ represents the j th column vector of \mathbf{A}_{k_i} . Further, it should be noted that the implication of $\mathbf{A}_{k_i,j}$ is different from that of $\mathbf{A}_{k_i}(l, j)$ used in Eq. (A21).

Finally, by using Eqs. (A21)–(A24), Eq. (25) yields

$$\begin{aligned} \text{EAF}_p(\mathbf{M}_k, l)^2 &= \sum_{i=1}^m \sum_{j=1}^{N-n} (\mathbf{B}_{k,p}^T \cdot \mathbf{A}_{k_i,j})^2 \\ &= \sum_{i=1}^m \sum_{j=1}^{(N-n)/d} (\mathbf{B}_{k',p-1}^T \cdot \mathbf{A}_{k'_i,j})^2 = \text{EAF}_{p-1}(\mathbf{M}_{k'}, l)^2 \end{aligned} \quad (\text{A27})$$

Appendix B: Equivalence of the two optimization models

In **Section 3.3**, the optimization model of an MCR(n, m) system with configuration specified by $k = \{k_i | i = 0, 1, \dots, m; k_i \in N^+ \cap [1, n]\}$ is given as

$$\min_{\mathbf{y}} \frac{1}{2} \|\mathbf{M}_k \cdot \mathbf{F}(\mathbf{y}) - \bar{\mathbf{H}}_k\|^2, \quad (\text{15})$$

where

$$\mathbf{F}(\mathbf{y}) = \begin{bmatrix} y_0 & y_1 & & y_{N-n-1} \\ y_1 & y_2 & & y_{N-n} \\ \vdots & \vdots & \cdots & \vdots \\ y_{n+1} & y_{n+2} & & y_N \end{bmatrix} \quad (9)$$

$$\mathbf{M}_k = [\lambda_k \mathbf{J}_k \quad -(1 + \lambda_k)], \quad (A7)$$

where $\lambda_k = (\lambda_{k_1}, \lambda_{k_2}, \dots, \lambda_{k_m})$ with

$$\lambda_{k_i} = \frac{k_i}{n+1} - 1$$

and \mathbf{J}_k is a matrix with size $m \times n$:

$$\mathbf{J}_k(i, j) = \begin{cases} 1, & j = k_i \\ 0, & j \neq k_i \end{cases}; i = 1, \dots, m; j = 1, \dots, n \quad (A8)$$

The expansion of Eq. (11) yields

$$[\lambda_k \mathbf{J}_k \quad -(1 + \lambda_k)] \cdot \begin{bmatrix} y_0 & y_1 & & y_{N-n-1} \\ y_1 & y_2 & & y_{N-n} \\ \vdots & \vdots & \cdots & \vdots \\ y_{n+1} & y_{n+2} & & y_N \end{bmatrix} \quad (A9)$$

$$= \begin{bmatrix} \bar{h}_{k_1,0} & \cdots & \bar{h}_{k_1,N-n-1} \\ \bar{h}_{k_2,0} & \cdots & \bar{h}_{k_2,N-n-1} \\ \vdots & \ddots & \vdots \\ \bar{h}_{k_m,0} & \cdots & \bar{h}_{k_m,N-n-1} \end{bmatrix}$$

For each measured $\bar{h}_{k_i,j}$, we have

$$\mathbf{M}_k(i) \cdot \begin{bmatrix} y_j \\ y_{j+1} \\ \vdots \\ y_{n+j+1} \end{bmatrix} = \bar{h}_{k_i,j}, \quad (A28)$$

where $\mathbf{M}_k(i) = [\lambda_{k_i} \mathbf{J}_k(i) \quad -(1 + \lambda_{k_i})]$ is the i th row of \mathbf{M}_k and $\mathbf{J}_k(i)$ is the i th row of \mathbf{J}_k . By extending Eq. (B1) by adding zeros to $\mathbf{M}_k(i)$,

$$[\mathbf{z}(j) \quad \mathbf{M}_k(i) \quad \mathbf{z}(N-n-j-2)] \cdot \begin{bmatrix} y_0 \\ y_1 \\ \vdots \\ y_N \end{bmatrix} \quad (A29)$$

$$= \bar{h}_{k_i,j}; j = 0, \dots, N-n-1; i = 1, \dots, m,$$

where $\mathbf{z}(n)$ represents a row vector containing n zeros. By integrating Eq. (B2) into a matrix form, we get

$$\begin{bmatrix} \mathbf{A}_{k_1} \\ \mathbf{A}_{k_2} \\ \vdots \\ \mathbf{A}_{k_m} \end{bmatrix} \cdot \mathbf{y} = \begin{bmatrix} \bar{\mathbf{h}}_{k_1}' \\ \bar{\mathbf{h}}_{k_2}' \\ \vdots \\ \bar{\mathbf{h}}_{k_m}' \end{bmatrix}, \quad (A30)$$

where $\bar{\mathbf{h}}_{k_i}' = \{\bar{h}_{k_i,0}, \bar{h}_{k_i,1}, \dots, \bar{h}_{k_i,N-n-1}\}^T$ is the transpose of the i th row vector of $\bar{\mathbf{H}}_k$ and

$$\mathbf{A}_{k_i}(j) = [\mathbf{z}(j) \quad \mathbf{M}_k(i) \quad \mathbf{z}(N-n-j-2)] \quad (A31)$$

or

$$\mathbf{A}_{k_i} = \begin{bmatrix} \lambda_{k_i} & 0 & \cdots & 1 & \cdots & 0 & \bar{\lambda}_{k_i} \\ & \lambda_{k_i} & 0 & \cdots & 1 & \cdots & 0 & \bar{\lambda}_{k_i} \\ & & \ddots & \ddots & \ddots & \ddots & & \ddots \\ & & & \lambda_{k_i} & 0 & \cdots & 1 & \cdots & 0 & \bar{\lambda}_{k_i} \end{bmatrix} \quad (17)$$

Finally, the restoration model can also be described as the model for finding the best value of vector \mathbf{y} to minimize the total error of Eq. (B2), as presented in Eq. (20).

$$\begin{cases} \min E = \frac{1}{2} \mathbf{U}_k^2 \\ \mathbf{U}_k = \begin{bmatrix} \mathbf{A}_{k_1} \\ \mathbf{A}_{k_2} \\ \vdots \\ \mathbf{A}_{k_m} \end{bmatrix} \cdot \mathbf{y} - \begin{bmatrix} \bar{\mathbf{h}}_{k_1}' \\ \bar{\mathbf{h}}_{k_2}' \\ \vdots \\ \bar{\mathbf{h}}_{k_m}' \end{bmatrix} \end{cases} \quad (21)$$

References

- [1] K.H. Oostermeijer, Review on short pitch rail corrugation studies, *Wear* 265 (9) (2008) 1231–1237.
- [2] S.L. Grassie, J. Kalousek, Rail corrugation: characteristics, causes, and treatments, *Proc. Inst. Mech. Eng. Part F* 207 (16) (2009) 57–68.
- [3] M. Hiensch, J.C.O. Nielsen, E. Verheijen, Rail corrugation in the Netherlands measurements and simulations, *Wear* 253 (1–2) (2002) 140–149.
- [4] W. Ping, W. Yuan, T. Huiyue, et al., Error theory of chord-based measurement system regarding track geometry and improvement by high frequency sampling, *Measurement* 115 (2) (2018) 204–216.
- [5] A. Haigermoser, B. Lubert, J. Rauh, G. Gräfe, Road and track irregularities: measurement, assessment and simulation, *Vehicle Syst. Dyn.* 53 (7) (2015) 878–957.
- [6] S. Iwnicki, T. Dahlberg, *Handbook of railway vehicle dynamics*, System (2006) 143–179.
- [7] M. Givoni, Development and impact of the modern high-speed train: a review, *Transp. Rev.* 26 (5) (2007) 593–611.
- [8] X. Sheng, C.J.C. Jones, D.J. Thompson, A theoretical model for ground vibration from trains generated by vertical track irregularities, *J. Sound Vib.* 272 (3–6) (2004) 937–965.
- [9] Jens Nielsen, Eric Berggren, Overview of Methods for Measurement of Track Irregularities Important for Ground-Borne Vibration, RIVAS CHALMERS WP2 Deliverable D2.5, 2013.
- [10] T. Karis, Track irregularities for high-speed trains (Master of Science Thesis), Stockholm, Sweden, 2009.
- [11] Akiyoshi Yoshimura, Study on theoretical foundations to restoring an original waveform of track irregularity and its application, *Proc. Jpn. Soc. Civ. Eng.* 1987 (377) (1987) 117–126.
- [12] A. Yoshimura, Y. Okumura, T. Anami, M. Kamiyama, A new method of repairing railway track irregularity using the restored waveform and its application, *Q. Rep. RTRI (Railway Tech. Res. Inst.) (Japan)* 38 (1) (1997) 13–18.
- [13] M. Kamiyama, A. Furukawa, A. Yoshimura, Theory and practice of optimum correction using restored track irregularity waveform, *Q. Rep. RTRI* 40 (2) (1999) 117–122.
- [14] S. Wang, Y. Xu, Y. Zhou, et al., Study of Rail Surface Irregularity Detection Based on Asymmetrical Chord Offset Method, in: *Third International Conference on Mechanic Automation and Control Engineering*, 2012, pp. 829–832.
- [15] K.U. Wolter, Reconstruction of Original Signals from Relative Measurement: EP, EP 1543439 A1, 2005.
- [16] S.L. Grassie, Measurement of railhead longitudinal profiles: a comparison of different techniques, *Wear* 191 (1–2) (1996) 245–251.
- [17] S.L. Grassie, Rail irregularities, corrugation and acoustic roughness: characteristics, significance and effects of reprofiling, *Proc. Inst. Mech. Eng., Part F* 226 (5) (2012) 542–557.
- [18] S.L. Grassie, M.J. Saxon, J.D. Smith, Measurement of longitudinal rail irregularities and criteria for acceptable grinding, *J. Sound Vib.* 227 (5) (1999) 949–964.
- [19] S.L. Grassie, Short wavelength rail corrugation: field trials and measuring technology, *Wear* 191 (1–2) (1996) 149–160.
- [20] S.L. Grassie, Rail corrugation: advances in measurement, understanding and treatment, *Wear* 258 (2005) 1224–1234.
- [21] P. Salvador, V. Naranjo, R. Insa, et al., Axlebox accelerations: Their acquisition and time-frequency characterisation for railway track monitoring purposes, *Measurement* 82 (2016) 301–312.
- [22] P. Salvador, V. Naranjo, R. Insa, P. Teixeira, Axlebox accelerations: their acquisition and time-frequency characterisation for railway track monitoring purposes, *Measurement* 82 (2016) 301–312.

- [23] M. Molodova, Z. Li, R. Dollevoet, Axle box acceleration: Measurement and simulation for detection of short track defects, *Wear* 271 (1–2) (2011) 349–356.
- [24] J.S. Lee, S. Choi, S.S. Kim, C. Park, Y.G. Kim, A mixed filtering approach for track condition monitoring using accelerometers on the axle box and bogie, *IEEE Trans. Instrum. Meas.* 61 (3) (2012) 749–758.
- [25] P. Aknin, H. Chollet, A new approach for the modelling of track geometry recording vehicles and the deconvolution of versine measurements. The dynamics of vehicles on roads and on tracks – supplement to vehicle system dynamics, volume 33, in: *Proceedings of the 16th IAVSD Symposium*; 1999 August 30–September 3, Pretoria (South Africa), 1999.
- [26] A. Yoshimura, Y. Naganuma, A novel method of reconstructing the railway track geometry using the particle filter, in: *The 10th World Congress on Railway Research*, 2013 November 24–27, Sydney, Australia.
- [27] B. Akpınar, E. Güllal, Railway track geometry determination using adaptive Kalman filtering model, *Measurement* 46 (1) (2013) 639–645.
- [28] X.J. Mao, H.F. Li, Y.D. Xu, A new method for detecting rail short wave irregularity, *Appl. Mech. Mater.* 361–363 (2013) 1640–1644.
- [29] A. Ben-Israel, T.N.E. Greville, *Generalized Inverses: Theory and Applications*, Wiley, 1974.
- [30] R.J. Marks (Ed.), *Advanced Topics in Shannon Sampling and Interpolation Theory*, Springer-Verlag, 1993.
- [31] A.C. Bidaud, *Railroad track geometry defect detector: US, US6347265*, 2002.
- [32] R.B. Lewis, A.N. Richards, A compensated accelerometer for the measurement of railway track crosslevel, *IEEE Trans. Veh. Technol.* 37 (3) (2002) 174–178.